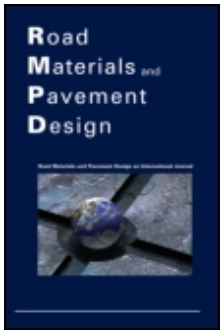

Rheological characterisation of cold bitumen emulsion slurries

Journal:	*Road Materials and Pavement Design*
Manuscript ID	RMPD-20-07-115.R1
Manuscript Type:	Special Issue
Keywords:	Bitumen emulsion, Viscosity, Rheology, Cold bitumen emulsion slurries, Dual Helical Ribbon, Maximum packing volume fraction

To cite this article:

Chiara Mignini, Davide Lo Presti, Gordon Airey & Andrea Graziani (2021) Rheological characterisation of cold bitumen emulsion slurries, Road Materials and Pavement Design, DOI: 10.1080/14680629.2021.1906303

Rheological characterisation of cold bitumen emulsion slurries

The performance of cold bitumen emulsion (CBE) mixtures is strongly linked to an optimised design of the binder blends and mastics. Hence type and dosages of bitumen, mineral additions but also their workability and compactability are key features to be characterised and optimised. This study aims at providing the scientific community with an approach for the fundamental characterisation of CBE materials by means of rotational viscometry. At first, a procedure for measuring the viscosity of CBE slurries using the Brookfield viscometer was investigated by comparing viscosity results obtained by using a traditional spindle geometry and a novel impeller engineered to avoid phase separation during testing: the dual helical ribbon. Afterwards, the effect of different types of mineral additions and bitumen emulsion was measured and modelled, as well as the influence of the overall solids concentration, to get useful information towards optimised design of CBE mixtures. The Krieger-Dougherty model proved to be a powerful tool to fit results and provide fundamental parameters for an improved engineering characterisation of CBE materials. Overall, the dual helical ribbon impeller was demonstrated to be a promising tool for the fundamental rheological characterisation of cold bitumen emulsion slurries.

Keywords: Bitumen emulsion, Viscosity, Rheology, Cold bitumen emulsion slurries, Dual Helical Ribbon, Maximum packing volume fraction

Introduction

In recent years, cold paving technologies are increasingly gaining attention as part of a progressive transition to a sustainable economic system. Cold mixtures and cold recycled mixtures allow diminishing pollutants emissions, energy consumption and raw materials use. They also lead to economic benefits, thanks to the consequent reduction of costs (Fang et al., 2016a).

Cold bitumen emulsion (CBE) mixtures are produced at ambient temperature. Therefore, bitumen, as it is, cannot be used as a binder and it is replaced with bitumen emulsion. Bitumen emulsion is a dispersion of bitumen droplets in water characterised by a much lower viscosity than bitumen, that makes it suitable for being used at ambient

temperatures. The emulsification process and the stability of the system are obtained through the use of emulsifiers (James, 2006). To compensate for the lack of heating, water is frequently added to improve the diffusion of the binder and promote the mixing and compaction operations (Grilli et al., 2012). Over time, breaking and setting of bitumen emulsion happens: bitumen droplets flocculate and coalesce, forming a thin film that coats the aggregate (James, 2006; Lesueur & Potti, 2004). Cementitious co-binders (e.g. ordinary Portland cement, fly ash, composite cement or ground granulated blast furnace slag) are often used to improve the mechanical properties of CBE materials. In this case, the hydration of the cementitious binder changes the microstructure of the material and can interact with emulsion breaking (Tan et al., 2014; Wang et al., 2013). CBE materials with both bitumen emulsion and cement may have an intermediate behaviour between those of hot mix asphalt (HMA) mixtures and cement-treated materials (Du, 2014; Graziani et al., 2020a). Bitumen emulsion breaking, cement hydration and water evaporation contribute to modifying the physical structure of CBE materials and improving their mechanical properties (Graziani et al., 2018; Miljković & Radenberg, 2014; Pouliot et al., 2003). This set of processes, known as curing, can take months or years before being totally completed (Du, 2018; Godenzoni et al., 2018; Mignini et al., 2019).

Despite the environmental benefits, doubts on CBE mixtures performance are still present, especially in upper pavement courses. These are mainly due to the need for a curing period before reaching a satisfactory mechanical response, combined with generally lower mechanical properties linked to the higher voids content of CBE mixtures compared to HMA mixtures (Graziani, et al., 2020a; Tebaldi et al., 2014; Xiao et al., 2018).

Most research activities studied CBE materials at the cured state or the curing process. Nevertheless, the awareness about CBE materials properties at the fresh state is fundamental. The workability of the fresh CBE materials, i.e. the response of the material to being mixed and laid, directly affect the volumetric and mechanical properties at the cured state (Kuchiishi et al., 2019; Raschia et al., 2019; Swiertz et al., 2012). However, direct measurement of the workability of mixtures is challenging (Hesami et al., 2012). Some researchers measured the torque needed to rotate a paddle in the mixtures at a certain speed (Gudimettla et al., 2004). In the study of HMA materials, a common practice is to use a multiscale approach (Underwood, 2015) to overcome these difficulties. The workability of HMA mixtures is, then, generally linked to its mastic or bitumen phase (Hesami et al., 2012; Sefidmazgi et al., 2013). In the study of CBE mixtures, the multiscale approach was lately used for predicting the mixture mechanical behaviour starting from the fine aggregate matrix mortar (Graziani et al., 2020b; Mignini et al., 2018; Mignini et al., 2021) or for supporting computational modelling (Fu et al., 2018). Studies on CBE mastics have been proposed for assessing the effect of mineral additions and their interaction with the bitumen emulsion on the rheological behaviour (Garilli et al., 2019; Godenzoni et al., 2017). Similarly to HMA materials, the workability at the scale of CBE mortars and mixtures is considered directly related to the rheological properties of the fresh mastic (Zhang et al., 2012). Then, the study of CBE slurries (or pastes), defined as the mastic at the fresh state, is quite common. CBE slurries are widely used for assessing the physical and mechanical properties of CBE mortars used in the construction of non-ballast tracks (Ouyang et al., 2017; Peng et al., 2014).

CBE slurries are complex fluids, composed of an aqueous phase, in which different solid particles, i.e. bitumen droplets and mineral additions, are dispersed. Solid

particles may have different dimensions: bitumen droplets range between 0.001 and 0.02 mm (James, 2006), whereas the mineral additions are ten times larger, ranging between 0.01 and 0.1 mm. The densities of the materials also differ significantly: water and bitumen are about three times lighter than mineral additions. Mixing mineral additions with the bitumen emulsion led to changing on its rheological response. Viscosity increases not only because of the presence of additional phases but also because of the beginning of phenomena such as emulsion breaking and cement hydration (Tan et al., 2014; Wang et al., 2013; Wang & Sha, 2010).

Aim of the study

This paper deals with the rheological characterisation of CBE slurries in terms of viscosity. The Brookfield viscometer was selected because of its user-friendliness, cost-effectiveness and good reliability. The experimental study was organised in two parts. The first focused on the definition of the testing procedure. The objective was selecting the most accurate methodology to investigate the viscosity of CBE slurries. Tests to define a simple testing procedure were carried out. In particular, the effect of using a traditional spindle and innovative Dual Helical Ribbon (DHR) impellers (Giancontieri et al., 2020) was assessed. The second part of the study focused on the effect of CBE slurries composition on the viscosity. A wide number of slurries was investigated to study and model the influence of bitumen emulsion and mineral additions. The study aims to provide useful information that can act as guidelines for defining the most effective CBE mixtures composition to obtain a good balance between their workability and their mechanical properties.

Review on viscosity measurement of cold bitumen emulsion slurries

Rheological studies for measuring the viscosity of complex fluids are a topic of interest in many industries, including road engineering and bituminous industry. A standard setup used for measuring the viscosity of bituminous materials is the rotational viscometer in coaxial cylinder configuration, e.g. Brookfield viscometer. In complex fluids, this instrument may not provide reliable measurements (Lo Presti et al., 2014). The difference in density of the components of the system, and the presence of processes altering the material structure (e.g. emulsion breaking and cement hydration in CBE slurries or swelling in crumb rubber modified bitumen) lead to a possible lack of sample stability, phase separation and tendency to sediment (Giancontieri et al., 2020). Then, the material can show a non-Newtonian and evolutive behaviour, that may affect viscosity measurements. For the reasons stated above, additional impellers have been proposed and developed for assisting the correct measurement of viscosity. Helical ribbon impellers were found to be the most suitable tool in the mixing of high-viscosity Newtonian and non-Newtonian fluids (Patterson et al., 1979; Yap et al., 1979). They have a pumping effect that helps maintain particles in suspension and confer a high shear deformation, improving the homogeneity of the system. On that basis, DHR impellers have been successfully developed for measuring the viscosity of crumb rubber modified binders and mastics (Astolfi et al., 2019; Medina et al., 2020). DHR allowed continuous measurement of viscosity guaranteeing the stability of the sample.

Despite the increasing interest in rheological characterisation of CBE slurries, standards for mixing and viscosity measurement procedures are not available. Many procedures have been proposed in the literature (Table 1). Mixing can be performed both through a mechanical mixer or hand-stirring. The mixing phase duration was generally limited to prevent the emulsion breaking and the cement hydration processes. Some Authors proposed an initial pre-mixing phase only of water and mineral additions.

This was intended to allow water to form a film around the surface of the mineral addition to hinder the instability of the emulsion and its premature breaking (Godenzoni et al., 2017; Ouyang & Tan, 2015).

The most common equipment for measuring the viscosity was the rheometer in coaxial cylinders configuration although the parallel plate configuration was also used. Tests were generally carried out at ambient temperature but also the effect of the changing in temperature was assessed (Zhang et al., 2012). Time zero of the testing was variable: it was either considered the first contact of water with cement (Fang et al., 2016b), or the instant immediately after the end of the mixing (Ouyang & Tan, 2015; Tan et al., 2014). In some studies, time zero was fixed at a selected time after the end of the mixing (Godenzoni et al., 2017; Zhang et al., 2012). In some experimental studies, before testing, a pre-shear mixing was applied to obtain a breakdown in the slurry structure and get uniform conditions (Ouyang & Tan, 2015; Tan et al., 2014). Some testing procedures involved rest periods or hysteresis cycles. These cycles allowed uniform testing conditions to be achieved thereby breaking the possible thixotropic structure to get more consistent measurements (Tan et al., 2014). Adopted shear rates were mainly linked to the equipment limits and were variable.

Viscosity measurement showed that CBE slurries have a non-Newtonian behaviour, generally showing a shear-thinning response (Fang et al., 2016b; Peng et al., 2014) although in some cases, it was followed by a shear-thickening response, suggesting a minimum flocculation shear rate (Ouyang et al., 2015). Different rheological behaviours were observed considering anionic or cationic emulsion. The anionic bitumen emulsion showed higher adsorption onto the surface of cement grains. This reduced the yield stress of the slurry and delayed the cement hydration process (Zhang et al., 2012). Slurries with plain emulsion had lower yield stress to resist

segregation than emulsion modified by viscosity modifying agent (Tan et al., 2014). Good stability of the emulsion helped to reduce the coalescence of bitumen droplets diminishing the viscosity (Tan et al., 2014). The nature of the mineral addition had a definite effect on the viscosity of CBE slurries. The addition of cement significantly increased viscosity compared to the impact of limestone filler (Fang et al., 2016b; Ouyang et al., 2017a) or calcium carbonate (Godenzoni et al., 2017). The breaking behaviour of the emulsion changed as a function of the mineral filler. In particular, using limestone filler, the main process was the bitumen droplets coalescence. Differently, when cement was added, a direct adhesion of the droplets on the surface of the cement occurred, due to its high adsorption ability (Ouyang et al., 2018). Moreover, the addition of cement highlighted a time-dependency starting within the first thirty testing minutes, that was not observed when cement was replaced with the limestone filler (Fang et al., 2016b).

The volumetric concentration also affected the rheological behaviour of CBE slurries: high solid particles volume fraction led to a higher viscosity and yield stress (Zhang et al., 2012). Water to cement ratio, emulsion to cement ratio, as well as particle sizes, significantly influenced the viscosity of the slurries (Garilli et al., 2016; Ouyang & Tan, 2015; Tan et al., 2014).

Table 1. Summary of the procedures proposed for mixing and viscosity testing of CBE slurries

Materials and methods

Materials

The CBE slurries investigated were obtained by mixing bitumen emulsion, mineral additions and deionised water. Two commercial cationic over-stabilised bitumen emulsions were adopted, both supplied by Valli Zabban S.p.A. Their designations are C60B10 and C60BP10 (EN 13808). Thus, both emulsions were produced with a residual bitumen content of 60%. The modification of the emulsion C60BP10 was obtained mixing plain bitumen and SBS latex. The density of both emulsions was 1.015 Mg/m^3. Two types of mineral additions were considered, specifically a finely ground limestone dust filler and a Portland limestone cement type II/B-LL with strength class 32.5R (EN 197-1). Table 2 reports the main physical properties of the mineral additions.

Table 2. Properties of mineral additions

Slurries composition

Table 3 summarises typical compositions of CBE mixtures in terms of bitumen, mineral additions and water content by mass of dry aggregates (Bocci et al., 2011; Dolzycki et al., 2017; Fang et al., 2016a). The corresponding values of the mass ratios are also reported. For each emulsion, 26 dispersions were investigated enclosing the CBE mixtures compositional ranges shown in Table 3. Four types of dispersions were considered:

- Bitumen emulsion and bitumen emulsion diluted with water
- Bitumen emulsion diluted with water plus limestone filler

- Bitumen emulsion diluted with water plus Portland cement
- Bitumen emulsion diluted with water plus limestone filler and Portland cement

Table 3. Typical composition of CBE mixtures derived from scientific literature

Table 4 summarises the composition of the investigated dispersions in terms of mass ratios and volume fraction. The latter was calculated as the ratio between the volume of the component and the total volume of the dispersion. The volume fraction of solid particles (φ_s) was calculated considering the bitumen and the mineral additions. All the tested slurries were obtained starting from the same liquid phase, bitumen emulsion diluted with water with a water/residual bitumen (W/B) ratio of 1.3, chosen as an intermediate value among the possible ratios.

Table 4. Composition by mass and volumetric fractions of tested bitumen emulsions and slurries

The CBE slurries were coded using a two-section alphanumeric code. The first section designates the components of the dispersion:

- Type of bitumen emulsion (B = plain bitumen, BP = modified bitumen)
- Dilution of water (W)
- Type of additions (F = limestone filler, C = Portland cement)

The second section defines the volume fraction of solid particles. For example, the code BWC_580 identifies a CBE slurry obtained by mixing bitumen emulsion produced with

plain bitumen, water and Portland cement with a concentration of the solid particles phase equal to 0.580.

Testing equipment and procedures

Mixing was carried out directly inside the Brookfield viscometer container both manually and mechanically. Firstly, water and mineral additions were stirred by hand for 10 s. The emulsion was then added and hand-stirred for 20 s. Finally, mechanical mixing was carried out at 100 rpm for 120 s using the impeller.

The viscosity was measured using two Brookfield DV-II PRO Digital viscometers: a low torque (LV model) and high torque (HA model) (Figure 1a). The LV model allows for testing low viscosity fluids (100% torque = 0.00006737 N m), the HA model is designed for medium-high viscous fluids (100% torque = 0.0014374 N m). The viscosity measurement accuracy, specified by the manufacturer, is 1% of the full-scale range.

Figure 1. Testing equipment a) Brookfield viscometer employed in the experimental study: LV model (on the left) and HA model (on the right) b) impellers used in the experimental study

The viscosity η measures the resistance to the flow of the materials and is defined as the ratio between the shear stress τ and shear rate $\dot{\gamma}$:

$$\eta = \frac{\tau}{\dot{\gamma}} \quad (1)$$

When η is measured employing a rotational viscometer in co-axial cylinder configuration $\dot{\gamma}$ varies at each point of the testing vessel. In the case of cylindrical geometry:

$$\dot{\gamma} = \frac{2\,\omega\,R_c^2\,R_s^2}{\chi^2(R_c^2 - R_s^2)}\cdot \quad (2)$$

$$\tau = \frac{T}{2\pi R_s^2 L} \quad (3)$$

where ω is the angular velocity of the impeller, R_c and R_s are the radius of the container and the impeller, respectively, T is the torque measured by the viscometer, χ is the radius at which $\dot{\gamma}$ is measured, and L is the effective length of the impeller.

Considering different geometries, Equations 2 and 3 are not valid anymore. Brookfield proposes to use an alternative method to determine an average value of $\dot{\gamma}$ based on the Metzner and Otto method (Lo Presti et al., 2014):

$$\dot{\gamma} = \mathrm{SRC}\cdot\ N = \mathrm{SRC}\left(\frac{60}{2\pi}\right)\omega \quad (4)$$

where N is the rotational speed, and SRC is the shear rate constant, linked to the impeller geometry.

Then, the apparent viscosity can be obtained as follows:

$$\eta = \frac{0.1}{N}\,T\% \cdot \mathrm{SMC}\cdot\ \mathrm{TK}\,\omega \quad (5)$$

where $T\%$ is the percentage of the maximum torque bearable by the viscometer, SMC is the spindle multiplier constant (function of the impeller geometry), TK is the torque constant, depending on the viscometer type (0.09373 and 2 for LV and HA model, respectively).

Two DHR impellers (DHR_2 and DHR_3) developed at the University of Nottingham (Medina et al., 2020) were used to measure the apparent viscosity of the dispersions. The results were compared to those obtained with the standard spindle S27 (Figure 1b). SMC values (Equation 5) are 11.5 and 9.5 for DHR_2, and DHR_3

respectively, and 25 for S27. The value of SRC (equation 4) is 0.34 for both impellers (Giancontieri et al., 2020). Measurements were performed at ambient temperature in controlled shear rate test modality. Three replicate specimens were tested for each dispersion.

Experimental programme

Figure 2 shows the organization of the experimental programme. Part 1, which considered the influence of both types of impellers (spindle and DHR) was organised in tasks.

Part 1A focused on evaluating the possible changes in the viscosity due to emulsion breaking or cement hydration. The task aimed to assure that the testing time scale is shorter than the structure-alteration time scale. During Part 1A, the viscosity of a selected number of slurries was measured at the constant speed of 100 rpm for 600 s, with a reading interval of 20 s (Figure 3a). Because CBE slurries are non-Newtonian materials, the measurement of the viscosity at different shear rates is crucial. Therefore, Part 1B focused on the effect of speed changes on the viscosity. As a starting point, the procedure suggested for bitumen and bitumen emulsion in EN 13302 and AASHTO T 316 were considered. In particular, EN 13302 considers a stabilising period before the reading of 30 s, whereas the reading period required by AASHTO 316 is 180 s. Procedures used in previous studies were considered, as well (Table 1). Figure 3b depicts the testing procedure followed during Part 1B. Starting from the mixing speed of 100 rpm, the test speed was changed every 180 s, and the torque was registered every 20 s. The task aimed at establishing an appropriate time for maintaining each test speed. This time must be long enough to allow the material stabilisation.

Figure 2. Experimental programme organization

Only the DHR impellers were used in Part 2. The selected stabilising period was 60 s. Thus, speed was changed once per 60 s, and the torque was recorded immediately before the speed switching. The first torque reading (time zero) was taken 180 s after the start of mechanical mixing (120 s of mixing + 60 s of stabilising period) at 100 rpm ($\dot{\gamma}$ = 34 s^{-1}). The procedures, depicted in Figure 3c and Figure 3d, had some slight differences between the LV and HA viscometer because of the different set of speeds available. When the LV model viscometer was used (Figure 3c), the test speed was gradually increased up to 200 rpm ($\dot{\gamma}$ = 68 s^{-1}) and then, decreased until reaching 50 rpm. For the HA model viscometer, the maximum speed is 100 rpm, and the set of testing speeds is reduced. Thus, after the first reading at 100 rpm, the speed was decreased until 50 rpm and, then, increased and decreased a second time (Figure 3d).

Figure 3. Test procedure followed during the experimental study a) Part1A, b) Part 1B, c) Part 2 - LV model viscometer, d) Part 2 - HA model viscometer

Results and discussion

Part 1: Definition of the testing procedure

The present section analyses the results obtained during the first part of the investigation. Figure 4 displays the results of Part 1A of the study. The curves of the average viscosity as a function of time were obtained at $\dot{\gamma}$ = 34 s^{-1} (100 rpm) with both types of impellers. Time zero in the x-axis coincides with the beginning of the mechanical mixing using the viscometer. The viscosity of the plain bitumen emulsion (B_596) measured with both S27 and DHR was almost constant within 600 s. The

viscosity obtained using different impellers was similar: the difference in the measured values was always lower than 10%. The outcome confirms that the SRC of S27 and DHR is the same from a practical point of view (Equation 4).

Figure 4. Viscosity changes over time of bitumen emulsion and CBE slurries measured using a) S27, b) DHR. Error bars represent the standard deviation of the experimental data.

The results obtained for systems characterised by a higher level of complexity, such as CBE slurries, highlighted some more variability. Some differences, due to the type of impeller, have been observed. The viscosity values measured with S27 (Figure 4a) showed some reliability issues in terms of repeatability (e.g. BWF_511 and BWC_511) and sample stability. Using S27, the viscosity of slurries increased with time when the filler was used. Also, for BWF_580 and BWFC_580, the test had to stop after 240 s because the torque was too high. Differently, when equipped with the DHR (Figure 4b), the viscometer was able of measuring the viscosity of these slurries over 600 s. This behaviour suggests that sedimentation and phase separation happened when using the standard spindle.

After the end of the first 120 s of measurement (mixing time), the viscosity of slurries measured with DHR can be considered constant: the variation of the viscosity between the measurement taken at 120 s and 600 s was lower than 15%. The only exception was for BWC_511, for which an increase of η of about 27% was measured. It is worth highlighting that the volumetric concentration of cement in this slurry is relatively high, and some change in the structure could have occurred. Indeed, after the hand mixing of a slurry characterised by cement volume fraction equal to 0.270 (BWC_580), sudden emulsion breaking occurred as displayed in

Figure 5a. Results showed that, in general, in the first minutes after the mixing, there was no evidence of variation in viscosity due to the emulsion breaking or the cement hydration. The viscosity change measured using S27 is ascribable to the instability of the sample and not to structural changes. Therefore, tests can be performed after a reasonable time after the mixing with no significative changes in the viscosity.

Figure 5. CBE slurries appearance: a) BWC_580 immediately after the hand-stirring (emulsion breaking), b) BPWF_680 right after the lowering of the impeller

Figure 6 reports the results of the tests carried out in Part 1B of the investigation. The average viscosity curves obtained using both S27 and DHR are depicted as a function of time and shear rate ($\dot{\gamma}$ = 6.8 - 68 s^{-1}). The x-axis zero (time zero) coincides with the start of the mechanical mixing. Results confirm that after the first 120 s (i.e. mixing time) the viscosity can be considered stabilised. S27 and DHR provided the same viscosity values for the plain bitumen emulsion, B_596 (Figure 6a). Also, the viscosity measurement with the S27 of slurries containing filler appeared less stable than those obtained with the DHR, showing a higher variability with time (Figure 6b and Figure 6d).

After the change of speed (and consequently of $\dot{\gamma}$), the viscosities of emulsion and CBE slurries were stabilised immediately with the DHR. When they were measured with S27, the stabilisation was slightly delayed. However, the viscosity measured after 60 s and 180 s were similar (difference lower than 10%). This suggests that the viscosity can be measured recording the torque percentage after 60 s from the speed change to reduce the total duration of the test. Tests carried out at $\dot{\gamma}$ = 6.8 s^{-1} (20 rpm) were not reliable. The speed was too low to avoid the sedimentation of the filler sized

particles. Therefore it is suggested that the viscosity measurement should be carried out at high shear rates (equal or greater than 17 s^{-1}).

Figure 6. Viscosity measured during Phase 1B a) B_596 (emulsion), b) BWF_511, c) BWC_437, d) BWFC_511. Error bars represent the standard deviation of the experimental data.

Part 2: Viscosity of CBE slurries

The present section displays the results obtained during Part 2 of the experimental plan using only the DHR impellers (DHR_2 and DHR_3). The choice to use DHR_2 or DHR_3 was made as a function of the predicted viscosity. DHR_3 is characterised by a narrower pitch, and it allows measuring lower viscosities, ranging between 0.01 Pa·s and 0.5 Pa·s. The viscosity range measurable by DHR_2 is 0.1 – 1 Pa·s. When both DHR_2 and DHR_3 could be used, the same viscosity values were obtained.

Figure 7 reports some examples of the hysteresis curves of the viscosity as a function of the shear rate. The "up" curves were obtained by increasing $\dot{\gamma}$ from 34 to 68 s^{-1} (from 100 to 200 rpm), whereas the "down" curves were measured after a successive decreasing of $\dot{\gamma}$ from 68 to 34 s^{-1}. Under the same speed, results obtained during the speed rising and decreasing measurement phases were very close. The difference in viscosity was always lower than 10% for $\dot{\gamma}$ ranging between 46 and 68 s^{-1}. When $\dot{\gamma}$ is smaller (34 s^{-1}) the difference was higher, reaching 64% for BWF_511. The outcome could be due to some kind of homogenisation of the material structure. This may be the result of an additional mixing due to the enhanced pumping effect obtained at the higher shear rates. In the analysis of the rheological behaviour, the down curves will be considered.

Figure 7. Viscosity as a function of shear rate measured during the rising phase of speed (up) and decreasing phase of speed (down) for a) B_596 and BWC_437, b) BWF_511 and BWFC_511, c) BP_596 and BPWC_437, d)BPWF_511 and BPWFC_511. Error bars represent the standard deviation of the experimental data.

Figure 8 reports the average viscosity flow curves measured with the DHR impellers for dispersions produced with the modified bitumen emulsion (BP). Results of dispersions produced with the plain bitumen emulsion (B) are not displayed as they were similar to those obtained with BP. In the adopted shear rate range, emulsion and its simple dilution with water had a Newtonian behaviour. This can be due to the small range of shear rate considered since the addition of a dispersed phase (i.e. bitumen) in a Newtonian fluid generally leads to a non-Newtonian behaviour. Differently, all the tested slurries were shear-thinning, indicating non-Newtonian behaviour.

The dilution of the emulsion with water reduced the viscosity significantly. Passing from W/B = 0.7 (BP_596) to 1.3 (BPW_425), η was about 250% lower. Considering slurries produced with the same mineral filler, increasing its dosage, and consequently the solid particles volume fraction, the viscosity always increased. The addition of cement increased the viscosity substantially when compared to slurries with the same total solid particles volume fraction and only filler (e.g. $\varphi_s = 0.511$).

Figure 8. Viscosity versus shear rate for a) BPW, b) BPWF, c) BPWC, d) BPWFC. Error bars represent the standard deviation of the experimental data.

BPWF_680 and BWF_700 (Table 4) were impossible to test.

Figure 5b shows BPWF_680 immediately after the hand stirring and the lowering of the impeller, which resulted in testing being unfeasible. The slurries had a shallow level of

fluidity with a doughy aspect. No impeller was able to measure the viscosity as the torque always exceeded 100%.

Figure 9 compares the viscosity measured in slurries with the same φ_s produced with the two emulsion types (B and BP). Results show that modified emulsion generally resulted in slurries with a slightly higher viscosity than plain bitumen emulsion, especially at high φ_s. Such a behaviour could be due to the presence of the SBS latex droplets in the modified emulsion that introduce an additional solid phase in the dispersion, and consequently, the actual value of φ_s is slightly higher.

Figure 9. Effect of bitumen emulsion type on the viscosity of bitumen emulsion dispersions and CBE slurries

Figure 10 reports viscosity results as a function of the solid particles volume fraction at $\dot{\gamma} = 34\ s^{-1}$. Such a shear rate value was selected because it is achievable using both the viscometers adopted and, at the same time, high enough to exclude particles sedimentation effects. The viscosity depends on the solid particle volume fraction: the viscosity grew as solid particles are added. This behaviour is typical of suspensions: at low concentrations, particles can move freely, and the suspension will be in a fluid, viscous state. Increasing the concentration of the solid particles, thus their volume fraction, they will develop an ever more packaged structure and the suspension will become a solid, elastic (Mason, 1999; Willenbacher & Georgieva, 2013). Starting from the Einstein model developed for suspensions of low volume fractions of spheres (diluted suspensions), several models were proposed to describe the dependence of the viscosity on the solid particles volume fraction, over the years (Barnes et al., 1989;

Mueller et al., 2010; Willenbacher & Georgieva, 2013). For concentrated suspensions, the relationship between the viscosity and the volume fraction must consider the maximum packing volume fraction φ_m. The latter represents the value at which the viscosity rises to infinite because a high level of particles packing is reached, such that the flow is impossible. Its value is connected to the particle size distribution and the particle shape, and to the inter-particle forces. In this paper, the Krieger-Dougherty model (Krieger & Dougherty, 1959), is considered for fitting the experimental data:

$$\eta = \eta_s\left(1 - \frac{\varphi_s}{\varphi_m}\right)^{-\eta_0 \varphi_m} \quad (6)$$

where η_s is the viscosity of the suspending medium, and η_0 is the intrinsic viscosity (also called Einstein coefficient). Curved lines in

Figure 10 represents the fitted model, whereas Table 5 reports the model parameters.

The values of φ_m depended on bitumen emulsion and mineral additive type. Dispersions produced with the modified bitumen emulsion had slightly lower values of φ_m confirming their higher viscosity compared to the viscosity of the dispersions with the plain bitumen (

Figure 10). Dispersions with only bitumen particles (i.e. BW and BPW) and those with only filler added (BWF and BPWF) had similar values of φ_m (from 0.678 to 0.690). When only cement is added (BWC and BPWC), φ_m diminished drastically (0.576 and 0.574), whereas the values of suspensions produced with both types of mineral additions (BWFC and BPWFC) where characterised by intermediate values (0.642 and 0.641). This effect could mainly be attributed to a different reactivity of the additions that can affect their interaction with the emulsion and the establishment of varying inter-particle forces. It could also be due to the different size and size distribution of the mineral addition, as well as their packability highlighted by different

Rigden voids (Table 2). Additionally, cement could have had a faster effect on the emulsion breaking leading to a change in the bitumen droplets dimension. Further studies are necessary to establish the contribution of the different phenomena. The obtained value of φ_m can also explain why BWF_700 and BPWF_680 (Table 4) were impossible to be tested. Indeed, the two selected φ_s are very close to the values of φ_m.

The η_s values showed a slight variation and were always higher with respect to the viscosity of the water at ambient temperature (about 0.001 Pa·s). This could be related to the choice of a too simple model considering the complexity of the system. Nevertheless, the model allowed a good fitting even for suspensions characterised by multiple solid particles types (i.e. bitumen, filler and cement) to be obtained.

Figure 10. Viscosity versus solid particles volume fraction a) B, b) BP (γ = 34 s^{-1})

Table 5. Krieger-Dougherty model parameters (Equation 6) obtained for all the tested materials

The product $(\eta_0\ \varphi_m)$, describing the growth rate of the viscosity, ranged between 0.973 and 1.446. Although slightly variable, its values are comprised in the range generally proposed in the rheology of suspensions (Barnes et al., 1989).

Figure 11 shows the relative viscosity ($\eta_r = \eta/\eta_s$) obtained by normalizing the viscosity experimental data with respect to the intrinsic viscosity obtained using the Krieger-Dougherty model (equation 6). η_r is shown as a function of the ratio between the solid particle volume fraction and the maximum packing volume fraction (φ_s/φ_m). All the materials show a similar behaviour: such evidence is confirmed by the comparable values of the model exponents, $\eta_0\ \varphi_m$. η_r increasing when adding solid

particles, and when a specific value of φ_s/φ_m was reached, it raised asymptotically. In general, the exponential increase started when φ_s/φ_m was between 0.85 and 0.95. When CBE slurries reached these concentration range values, the solid particles did not flow freely anymore, and it could be assumed that a packed concentrated structure was formed (Figure 11). It is worth highlighting that the viscosity growth could also be related to the starting of other phenomena due to the interaction of the two co-binders (i.e. emulsion breaking or cement hydration). Again, further studies are needed to provide a better explanation of such outcomes.

Figure 11. Relative viscosity as a function of the ratio between solid particles volume fraction and maximum packing volume fraction

Conclusions

This paper developed a robust procedure for measuring the viscosity of CBE slurries using a rotational viscometer. Measurements carried out using a novel Dual Helical Ribbon (DHR) impeller and a standard spindle, proved that the DHR allowed more reliable results to be obtained, diminishing the phase separation and sedimentation effects. Following the testing procedure developed, the study focused on evaluating the impact of different mineral additions and bitumen types on the viscosity of CBE slurries. Also, the influence of solid particles concentrations was evaluated to obtain useful information for CBE mixtures composition design. As expected, CBE slurries were non-Newtonian, showing a shear-thinning behaviour within the tested shear rate range. A small difference was observed due to the bitumen emulsion type: with modified bitumen, the viscosity was slightly higher at the same solid particles volume fractions. The type of addition had a substantial effect on the viscosity. When only

Portland cement was used, the viscosity was significantly higher than those of slurries produced with only limestone filler. Slurries produced with both additions exhibited an intermediate behaviour. Despite the high complexity of the system, the Krieger-Dougherty model provided a good fitting of the experimental data, allowing the identification of the maximum packing volume fraction. It was found that when 95% of the maximum packing volume fraction is reached, the viscosity starts rapidly increasing, suggesting the formation of a packed structure. Overall, the use of rotational viscometry with DHR geometry demonstrated to be a promising approach for the fundamental rheological characterisation of cold bitumen emulsion slurries.

Further studies are needed to assess the effectiveness of using the DHR, for example, investigating more significant ranges of shear rates. To this aim, the application of the DHR in Dynamic Shear Rheometers is currently under investigation. The study of the effect of mineral additions types, bitumen emulsion types and solid particles concentration merits being explored, as well as the impact of particle sizes and their distribution should be evaluated. Additional studies are required to relate the viscosity of CBE slurries and fresh properties of CBE mixtures to obtain a practical recommendation to accurately define the composition of the mixtures.

Acknowledgements

Declaration of interest statement

The authors declare no conflict of interest.

Contribution of the authors

References

Astolfi, A., Subhy, A., Praticò, F., & Lo Presti, D. (2019). *Quality-control procedure for dry-process rubberised asphalt mastics*. 560–567. https://doi.org/10.1201/9781351063265-75

Barnes, H. A., Hutton, J. F., & Walters, K. (1989). An introduction to rheology (Vol. 3). Elsevier. *Elsevier*.

Bocci, M., Grilli, A., Cardone, F., & Graziani, A. (2011). A study on the mechanical behaviour of cement-bitumen treated materials. *Construction and Building Materials*, *25*(2), 773–778. https://doi.org/10.1016/j.conbuildmat.2010.07.007

Dolzycki, B., Jaczewski, M., & Szydlowski, C. (2017). The long-term properties of mineral-cement-emulsion mixtures. *Construction and Building Materials*. https://doi.org/10.1016/j.conbuildmat.2017.09.032

Du, S. (2014). Interaction mechanism of cement and asphalt emulsion in asphalt emulsion mixtures. *Materials and Structures/Materiaux et Constructions*, *47*(7), 1149–1159. https://doi.org/10.1617/s11527-013-0118-1

Du, S. (2018). Effect of curing conditions on properties of cement asphalt emulsion mixture. *Construction and Building Materials*, *164*, 84–93. https://doi.org/10.1016/j.conbuildmat.2017.12.179

Fang, X., Garcia-Hernandez, A., & Lura, P. (2016a). Overview on cold cement bitumen emulsion asphalt. *RILEM Technical Letters*, *1*(December), 116. https://doi.org/10.21809/rilemtechlett.2016.23

Fang, X., Garcia-Hernandez, A., Winnefeld, F., & Lura, P. (2016b). Influence of cement on rheology and stability of rosin emulsified anionic bitumen emulsion. *Journal of Materials in Civil Engineering*, *28*(5), 1–12.

https://doi.org/10.1061/(ASCE)MT.1943-5533.0001454

Fu, J., Yang, Y., Zhang, X., & Wang, F. (2018). Different strain distributions of cement-emulsified asphalt concrete pavement between the macro- and meso-scale. *Road Materials and Pavement Design*. https://doi.org/10.1080/14680629.2016.1259121

Garilli, E., Autelitano, F., & Giuliani, F. (2019). Use of bending beam rheometer test for rheological analysis of asphalt emulsion-cement mastics in cold in-place recycling. *Construction and Building Materials*, *222*, 484–492. https://doi.org/10.1016/j.conbuildmat.2019.06.141

Garilli, E., Autelitano, F., Godenzoni, C., Graziani, A., & Giuliani, F. (2016). Early age evolution of rheological properties of over-stabilized bitumen emulsion-cement pastes. *Construction and Building Materials*, *125*, 352–360. https://doi.org/10.1016/j.conbuildmat.2016.08.054

Giancontieri, G., Hargreaves, D., & Lo Presti, D. (2020). Are we correctly measuring the rotational viscosity of heterogeneous bituminous binders? *Road Materials and Pavement Design*, *0*(0), 1–20. https://doi.org/10.1080/14680629.2020.1724559

Godenzoni, C., Bocci, M., & Graziani, A. (2017). Rheological characterization of cold bituminous mastics produced with different mineral additions. *Transport Infrastructure and Systems - Proceedings of the AIIT International Congress on Transport Infrastructure and Systems, TIS 2017*, *2015*, 185–191. https://doi.org/10.1201/9781315281896-26

Godenzoni, C., Graziani, A., Bocci, E., & Bocci, M. (2018). The evolution of the mechanical behaviour of cold recycled mixtures stabilised with cement and bitumen: field and laboratory study. *Road Materials and Pavement Design*. https://doi.org/10.1080/14680629.2017.1279073

Graziani, A., Iafelice, C., Raschia, S., Perraton, D., & Carter, A. (2018). A procedure for characterizing the curing process of cold recycled bitumen emulsion mixtures. *Construction and Building Materials*, *173*, 754–762. https://doi.org/10.1016/j.conbuildmat.2018.04.091

Graziani, A., Mignini, C., Bocci, E., & Bocci, M. (2020a). Complex Modulus Testing and Rheological Modeling of Cold-Recycled Mixtures. *Journal of Testing and Evaluation*, *48*(1), 20180905. https://doi.org/10.1520/jte20180905

Graziani, A., Raschia, S., Mignini, C., & Carter, A. (2020b). Use of fine aggregate matrix to analyze the rheological behavior of cold recycled materials. *Materials and Structures*, *7*. https://doi.org/10.1617/s11527-020-01515-7

Grilli, A., Graziani, A., & Bocci, M. (2012). *Compactability and thermal sensitivity of cement – bitumen-treated materials*. *May 2013*, 37–41. https://doi.org/10.1080/14680629.2012.742624

Gudimettla, J. M., Cooley, L. A., & Brown, E. R. (2004). Workability of hot-mix asphalt. *Transportation Research Record*. https://doi.org/10.3141/1891-27

Hesami, E., Jelagin, D., Kringos, N., & Birgisson, B. (2012). An empirical framework for determining asphalt mastic viscosity as a function of mineral filler concentration. *Construction and Building Materials*, *35*, 23–29. https://doi.org/10.1016/j.conbuildmat.2012.02.093

James, A. (2006). Overview of asphalt emulsion. *Transportation Research Circular*, 1–15. https://doi.org/10.17226/23246

Krieger, I. M., & Dougherty, T. J. (1959). A Mechanism for Non-Newtonian Flow in Suspensions of Rigid Spheres. *Transactions of the Society of Rheology*. https://doi.org/10.1122/1.548848

Kuchiishi, A. K., Vasconcelos, K., & Bariani Bernucci, L. L. (2019). Effect of mixture

composition on the mechanical behaviour of cold recycled asphalt mixtures. *International Journal of Pavement Engineering*. https://doi.org/10.1080/10298436.2019.1655564

Lesueur, D., & Potti, J. J. (2004). Cold mix design: A rational approach based on the current understanding of the breaking of bituminous emulsions. *Road Materials and Pavement Design*, *5*(X), 65–87. https://doi.org/10.1080/14680629.2004.9689988

Lo Presti, D., Fecarotti, C., Clare, A. T., & Airey, G. (2014). Toward more realistic viscosity measurements of tyre rubber-bitumen blends. *Construction and Building Materials*, *67*(PART B), 270–278. https://doi.org/10.1016/j.conbuildmat.2014.03.038

Mason, T. G. (1999). New fundamental concepts in emulsion theology. *Current Opinion in Colloid and Interface Science*, *4*(3), 231–238. https://doi.org/10.1016/S1359-0294(99)00035-7

Medina, J. G., Giancontieri, G., & Lo Presti, D. (2020). Quality control of manufacturing and hot storage of crumb rubber modified binders. *Construction and Building Materials*, *233*, 117351. https://doi.org/10.1016/j.conbuildmat.2019.117351

Mignini, C., Cardone, F., & Graziani, A. (2018). Experimental study of bitumen emulsion–cement mortars: mechanical behaviour and relation to mixtures. *Materials and Structures/Materiaux et Constructions*, *51*(6). https://doi.org/10.1617/s11527-018-1276-y

Mignini, C., Cardone, F., Graziani, A., Morbi, A., & Setti, L. (2019). Effect of curing on the indirect tensile failure energy of cement-bitumen treated materials. In *Bituminous Mixtures and Pavements VII*. https://doi.org/10.1201/9781351063265-

32

Mignini, Chiara, Cardone, F., & Graziani, A. (2021). Using fine aggregate matrix mortars to predict the curing behaviour of cement bitumen treated materials produced with different cements. *Construction and Building Materials*, *268*, 121201. https://doi.org/10.1016/j.conbuildmat.2020.121201

Miljković, M., & Radenberg, M. (2014). Fracture behaviour of bitumen emulsion mortar mixtures. *Construction and Building Materials*, *62*, 126–134. https://doi.org/10.1016/j.conbuildmat.2014.03.034

Mueller, S., Llewellin, E. W., & Mader, H. M. (2010). The rheology of suspensions of solid particles. *Proceedings of the Royal Society A: Mathematical, Physical and Engineering Sciences*. https://doi.org/10.1098/rspa.2009.0445

Ouyang, J., Hu, L., Li, H., & Han, B. (2018). Effect of cement on the demulsifying behavior of over-stabilized asphalt emulsion during mixing. *Construction and Building Materials*, *177*, 252–260. https://doi.org/10.1016/j.conbuildmat.2018.05.141

Ouyang, J., Li, H., & Han, B. (2017a). The rheological properties and mechanisms of cement asphalt emulsion paste with different charge types of emulsion. *Construction and Building Materials*, *147*, 566–575. https://doi.org/10.1016/j.conbuildmat.2017.04.201

Ouyang, J., & Tan, Y. (2015). Rheology of fresh cement asphalt emulsion pastes. *Construction and Building Materials*, *80*, 236–243. https://doi.org/10.1016/j.conbuildmat.2015.01.078

Ouyang, J., Tan, Y., Corr, D. J., & Shah, S. P. (2016). Investigation on the mixing stability of asphalt emulsion with cement through viscosity. *Journal of Materials in Civil Engineering*, *28*(12), 1–8. https://doi.org/10.1061/(ASCE)MT.1943-

5533.0001657

Ouyang, J., Tan, Y., Corr, D. J., & Shah, S. P. (2017b). Viscosity prediction of fresh cement asphalt emulsion pastes. *Materials and Structures/Materiaux et Constructions*, *50*(1), 1–10. https://doi.org/10.1617/s11527-016-0897-2

Ouyang, J., Tan, Y., Li, Y., & Zhao, J. (2015). Demulsification process of asphalt emulsion in fresh cement-asphalt emulsion paste. *Materials and Structures/Materiaux et Constructions*, *48*(12), 3875–3883. https://doi.org/10.1617/s11527-014-0446-9

Patterson, W. I., Carreau, P. J., & Yap, C. Y. (1979). Mixing with helical ribbon agitators: Part II. Newtonian Fluids. *AIChE Journal*. https://doi.org/10.1002/aic.690250317

Peng, J., Deng, D., Liu, Z., Yuan, Q., & Ye, T. (2014). Rheological models for fresh cement asphalt paste. *Construction and Building Materials*, *71*, 254–262. https://doi.org/10.1016/j.conbuildmat.2014.08.031

Pouliot, N., Marchand, J., & Pigeon, M. (2003). Hydration mechanisms, microstructure, and mechanical properties of mortars prepared with mixed binder cement slurry-asphalt emulsion. *Journal of Materials in Civil Engineering*, *15*(1), 54–59. https://doi.org/10.1061/(ASCE)0899-1561(2003)15:1(54)

Raschia, S., Mignini, C., Graziani, A., Carter, A., Perraton, D., & Vaillancourt, M. (2019). Effect of gradation on volumetric and mechanical properties of cold recycled mixtures (CRM). *Road Materials and Pavement Design*, *20*(sup2), S740–S754. https://doi.org/10.1080/14680629.2019.1633754

Sefidmazgi, N. R., Teymourpour, P., & Bahia, H. U. (2013). Effect of particle mobility on aggregate structure formation in asphalt mixtures. *Road Materials and Pavement Design*. https://doi.org/10.1080/14680629.2013.812844

Swiertz, D., Johannes P. Tashman, L., & Bahia, H. (2012). Evaluation of laboratory coating and compaction procedures for cold mix asphalt. *Asphalt Paving Technology-Proceedings Association of Asphalt Technologists*, *81*, 81.

Tan, Y., Ouyang, J., & Li, Y. (2014). Factors influencing rheological properties of fresh cement asphalt emulsion paste. *Construction and Building Materials*, *68*, 611–617. https://doi.org/10.1016/j.conbuildmat.2014.07.020

Tebaldi, G., Dave, E. V., Marsac, P., Muraya, P., Hugener, M., Pasetto, M., Graziani, A., Grilli, A., Bocci, M., Marradi, A., Wendling, L., Gaudefroy, V., Jenkins, K., Loizos, A., & Canestrari, F. (2014). Synthesis of standards and procedures for specimen preparation and in-field evaluation of cold-recycled asphalt mixtures. *Road Materials and Pavement Design*. https://doi.org/10.1080/14680629.2013.866707

Underwood, B. S. (2015). Multiscale modeling approach for asphalt concrete and its implications on oxidative aging. In *Advances in asphalt materials* (pp. 273–302). Woodhead Publishing.

Wang, F., Liu, Y., & Hu, S. (2013). Effect of early cement hydration on the chemical stability of asphalt emulsion. *Construction and Building Materials*, *42*, 146–151. https://doi.org/10.1016/j.conbuildmat.2013.01.009

Wang, Z., & Sha, A. (2010). Micro hardness of interface between cement asphalt emulsion mastics and aggregates. *Materials and Structures/Materiaux et Constructions*, *43*(4), 453–461. https://doi.org/10.1617/s11527-009-9502-2

Willenbacher, N., & Georgieva, K. (2013). Rheology of Disperse Systems. *Product Design and Engineering: Formulation of Gels and Pastes*, 7–49. https://doi.org/10.1002/9783527654741.ch1

Xiao, F., Yao, S., Wang, J., Li, X., & Amirkhanian, S. (2018). A literature review on

cold recycling technology of asphalt pavement. *Construction and Building Materials*, *180*, 579–604. https://doi.org/10.1016/j.conbuildmat.2018.06.006

Yap, C. Y., Patterson, W. I., & Carreau, P. J. (1979). Mixing with helical ribbon agitators: Part III. Non-Newtonian fluids. *AIChE Journal*. https://doi.org/10.1002/aic.690250318

Zhang, Y., Kong, X., Hou, S., Liu, Y., & Han, S. (2012). Study on the rheological properties of fresh cement asphalt paste. *Construction and Building Materials*, *27*(1), 534–544. https://doi.org/10.1016/j.conbuildmat.2011.07.010

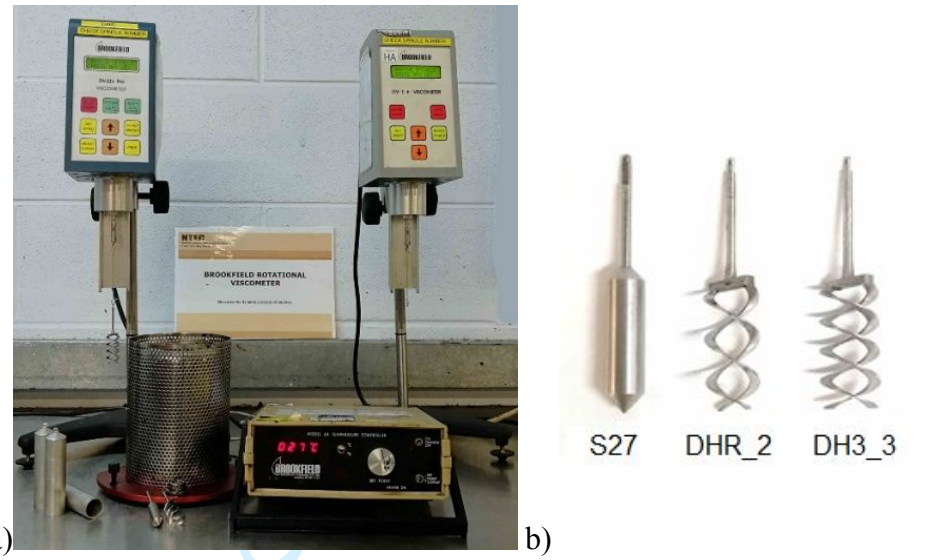

a) b)

Figure 1. Testing equipment a) Brookfield viscometer employed in the experimental study: LV model (on the left) and HA model (on the right) b) impellers used in the experimental study

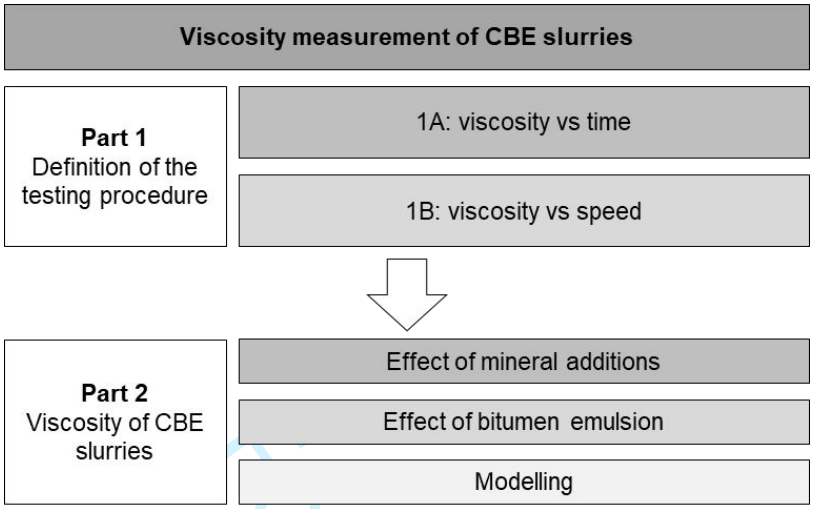

Figure 2. Experimental programme organization

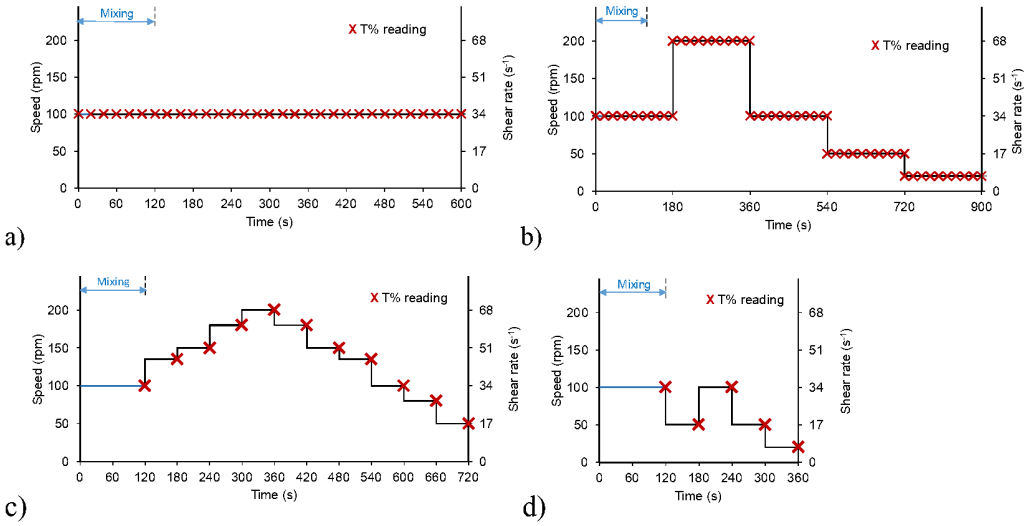

Figure 3. Test procedure followed during the experimental study a) Part1A, b) Part 1B, c) Part 2 - LV model viscometer, d) Part 2 - HA model viscometer

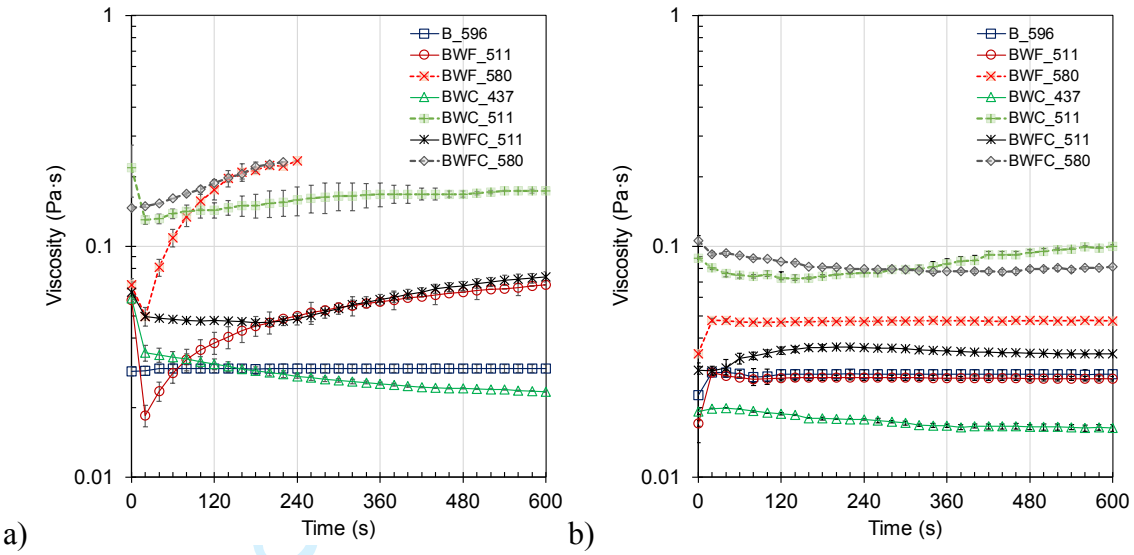

Figure 4. Viscosity changes over time of bitumen emulsion and CBE slurries measured using a) S27, b) DHR. Error bars represent the standard deviation of the experimental data.

a)  b) 

Figure 5. CBE slurries appearance: a) BWC_580 immediately after the hand-stirring (emulsion breaking), b) BPWF_680 right after the lowering of the impeller

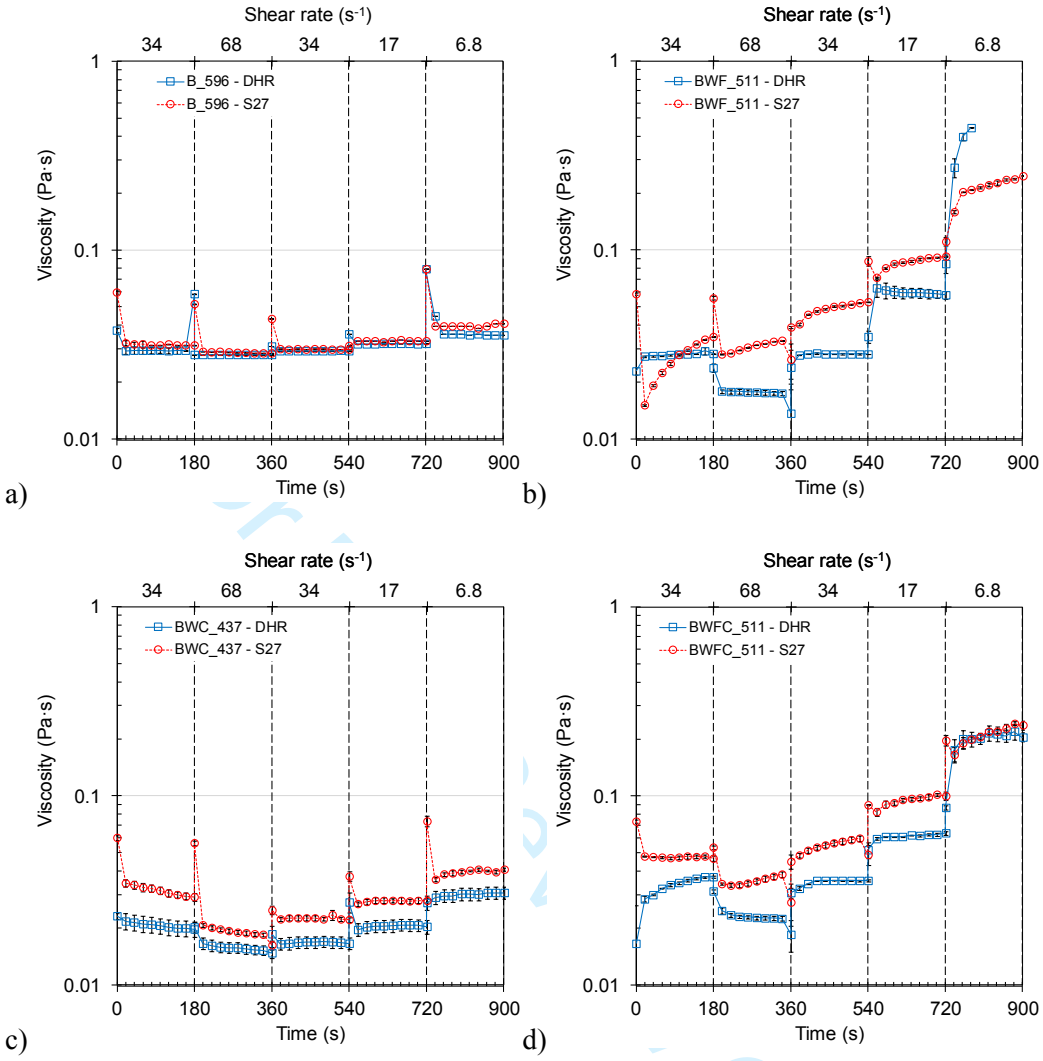

Figure 6. Viscosity measured during Phase 1B a) B_596 (emulsion), b) BWF_511, c) BWC_437, d) BWFC_511. Error bars represent the standard deviation of the experimental data.

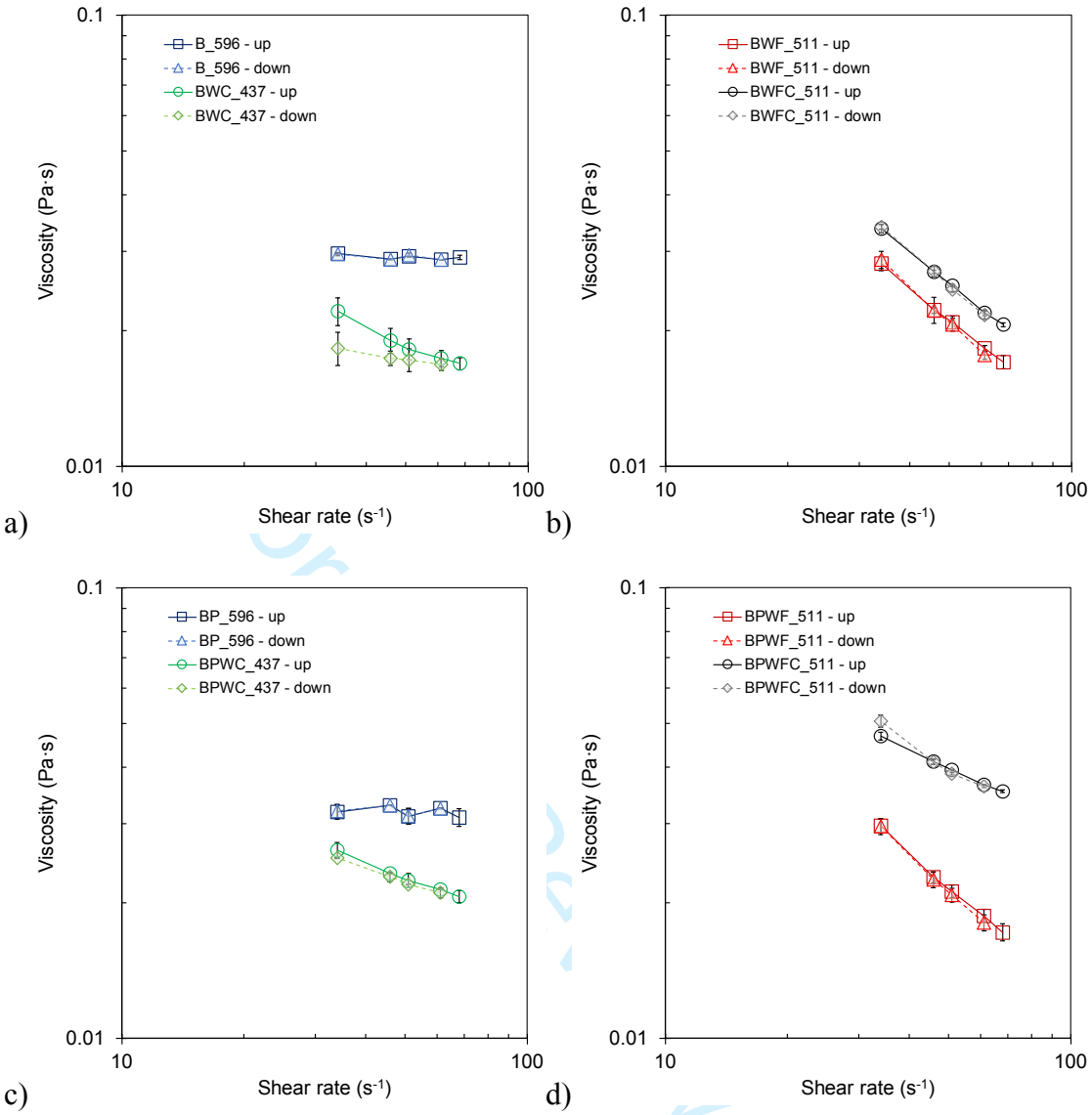

Figure 7. Viscosity as a function of shear rate measured during the rising phase of speed (up) and decreasing phase of speed (down) for a) B_596 and BWC_437, b) BWF_511 and BWFC_511, c) BP_596 and BPWC_437, d)BPWF_511 and BPWFC_511. Error bars represent the standard deviation of the experimental data.

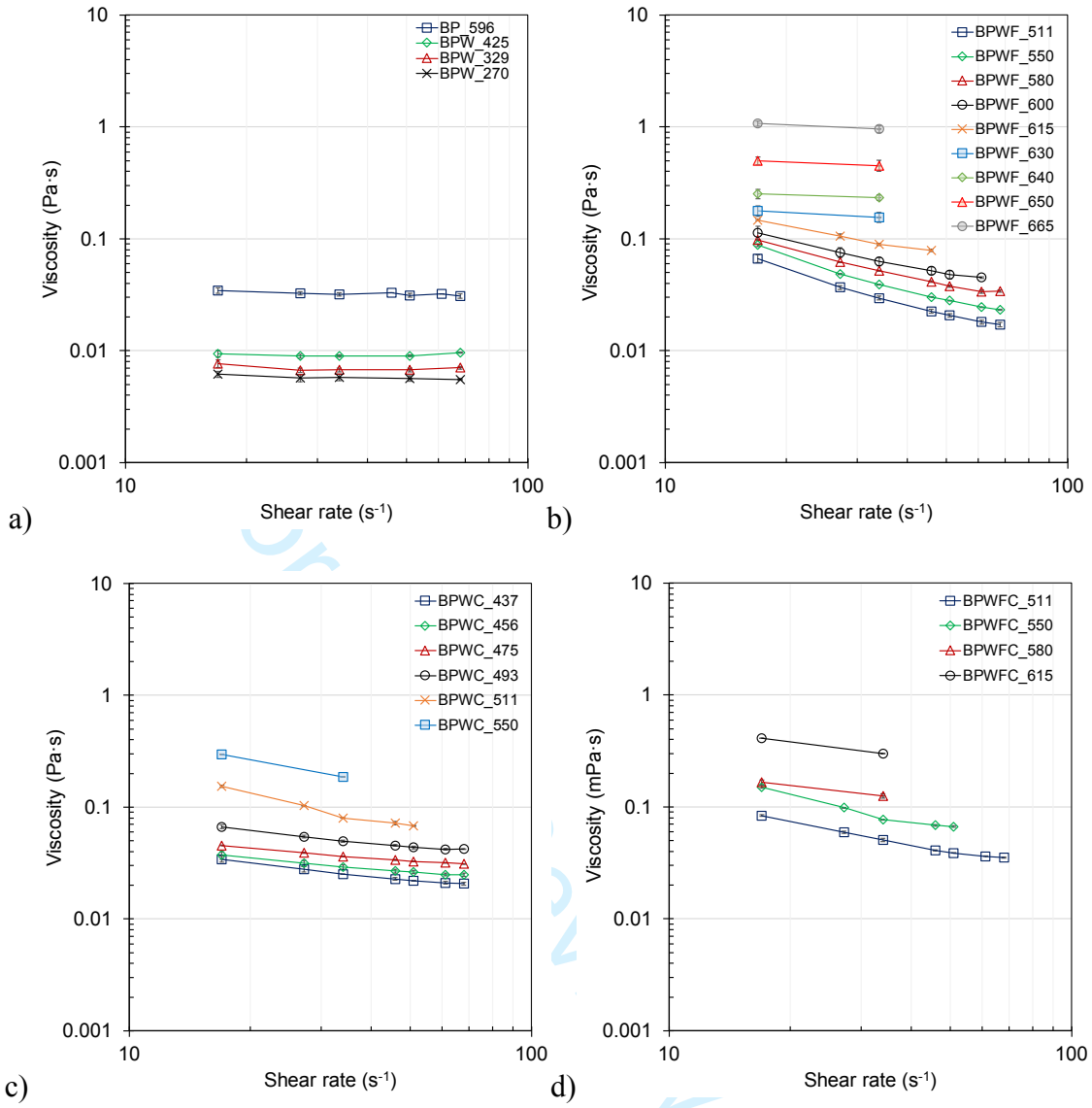

Figure 8. Viscosity versus shear rate for a) BPW, b) BPWF, c) BPWC, d) BPWFC. Error bars represent the standard deviation of the experimental data.

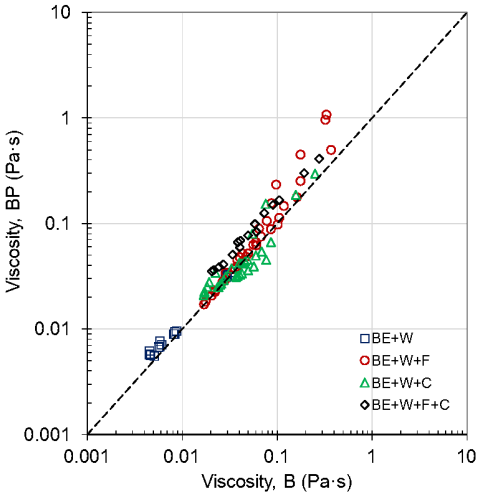

Figure 9. Effect of bitumen emulsion type on the viscosity of bitumen emulsion dispersions and CBE slurries

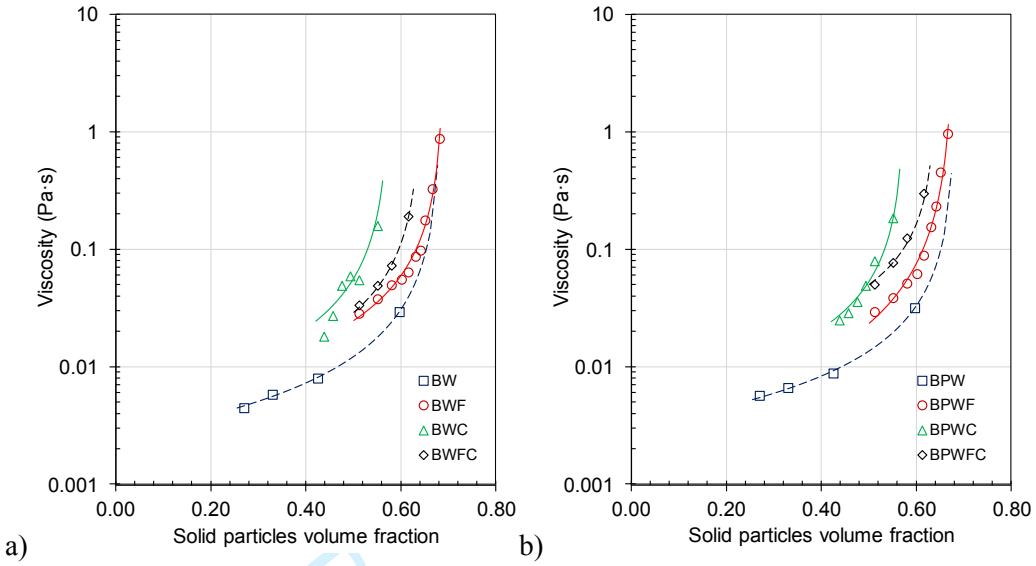

Figure 10. Viscosity versus solid particles volume fraction a) B, b) BP (γ = 34 s-1)

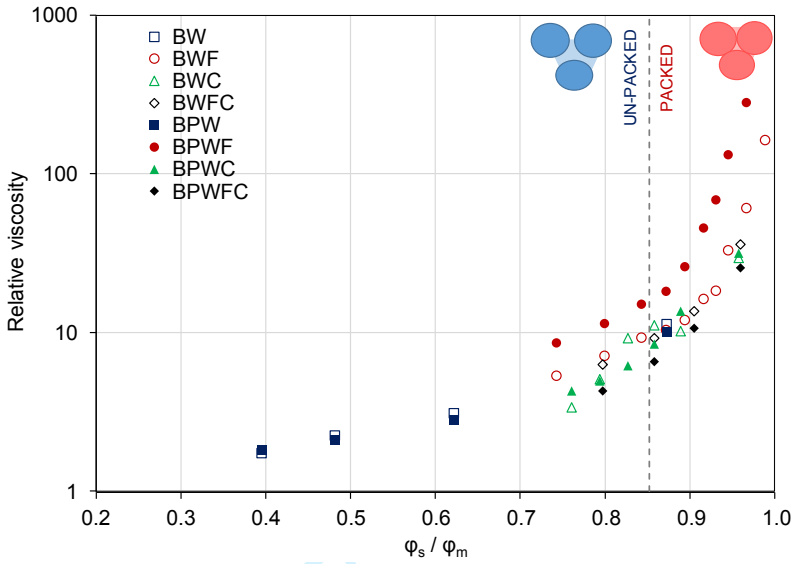

Figure 11. Relative viscosity as a function of the ratio between solid particles volume fraction and maximum packing volume fraction

Table 1. Summary of the procedures proposed for mixing and viscosity testing of CBE slurries

Reference	Mixing procedure	Viscosity measurement	
		Equipment	**Procedure**
Zhang et al., 2012	Water and emulsion added into the mixer. Cement gradually introduced within 2 min at 62 rpm. 10 s stop interval and mixing for 2 min at 125 rpm	Brookfield viscometer	Tested at different temperatures and times after mixing. Before testing slurry kept in a mixing bowl covered with a soaked towel, then remixed at 62 rpm for 30 s.
Peng et al., 2014	Water and emulsion stirred into a mixer for 1 min at 62 rpm. Cement introduced within 0.5 min at 62 rpm. Mixing for 2 min at 125 rpm and 0.5 min at 62 rpm	Rotary rheometer in coaxial cylinder configuration	Tested 5 min after mixing. Shear rate 1-300 s^{-1}. Up-curve/constant/down curve (down curve considered for the analysis).
Tan et al., 2014	n.a.*	Parallel plate rheometer	Immediately tested. Pre-shear at 50 s^{-1} for 60 s. Linear decreasing shear rate from 50 - 0 s^{-1} for 10 s. 60 s or 300 s of rest. Two hysteresis cycles within 2 min, 0-50 s^{-1} (up curves of the second cycle considered in the analysis).
Ouyang et al., 2015	n.a.*	Parallel plate rheometer	Immediately tested at 20 s^{-1}. Before each test, additional hand-stirring. Increasing shear rates from 2 to 50 s^{-1} within 60 s. Each step lasted 30 s. Test at 20 s^{-1} until the loss of fluidity.
Ouyang et al., 2016; Ouyang & Tan, 2015	Hand-stirring. Cement and water stirred firstly for 2 min, then emulsion added and continually stirred for 2 min.	Rheometer in coaxial cylinder geometry	Sample immediately loaded (within 1 min from mixing). 2 min pre-shear at 300 s^{-1} and 2 min of rest. Then strain rate increased gradually over 1 min to a final value of 100 s^{-1}.
Garilli et al., 2016	Water and cement and stirred for 1 min. Emulsion added and stirred for 2 min.	Rheometer in coaxial cylinder configuration	Linear shear stress ramp from 0 to 50 Pa, 5s duration of each stress step. Time zero: 10 min after water addition. Test every 15 min until the loss of fluidity.
Fang et al., 2016b	Filler and cement premixed. Addition of emulsion, mixing at 60 rpm for 1 min.	Brookfield viscometer, spindle S27	Sample poured into the container and tested immediately. Time zero: coincident with the cement addition.
Ouyang et al., 2017a	n.a.*	Rheometer in coaxial cylinder geometry	Immediately testing. 2 min pre-shear at 300 s^{-1}. 2 min rest. Shear rate is decreased from 100 s^{-1} to 1 s^{-1}.
Ouyang et al., 2018; Ouyang et al., 2017b	Same used in: Ouyang et al., 2016; Ouyang & Tan, 2015	Rheometer in coaxial cylinder geometry	Immediately sheared. Up/down/up curve, linearly increasing shear rate from 0 to 100 s^{-1}, each curve within 1 min (second up curve considered in the analysis).
Godenzoni et al., 2017	Mixing of mineral filler and water. Addition of emulsion and hand-stirring. Mixing at 489 rpm with a high-shear mixer.	Brookfield viscometer, spindle S21	Test after 15, 45 and 60 min from the beginning of the mechanical mixing. Shear rate from 50 up to 200 s^{-1}

* information about the procedure not available

Table 2. Properties of mineral additions

		Filler	**Cement**
Property	Test standard	Nominal value	Nominal value
Particle density (Mg/m^3)		2.650	3.020
Maximum dimension (mm)		0.125	0.090
Blaine surface area (cm^2/g)	EN 196-6	3400	3800
Rigden voids (%)	EN 1097-4	23.8	33.2

Table 3. Typical composition of CBE mixtures derived from scientific literature

CBE mixtures typical composition		
Component	Lower limit By mass (%)	Upper limit By Mass (%)
Residual bitumen (B)	1.8	3.0
Cement (C)	0.0	6.0
Filler (F)	5.0	10.0
Water (W)	3.0	6.0
CBE mixtures typical mass ratios		
Ratios	Lower limit Mass ratio	Upper limit Mass ratio
Residual bitumen/Cement (B/C)	0.3	
Residual bitumen/Filler (B/F)	0.18	0.60
Cement/Filler (C/F)	0	0.60
Water/Residual bitumen (W/B)	0.56	1.67
Water/Cement (W/C)	1.00	
Water/Filler (W/F)	0.30	1.00

Table 4. Composition by mass and volumetric fractions of tested bitumen emulsions and slurries

Mass ratio					Volume fraction					Density
B/F	B/C	W/B	W/F	W/C	W	B	F	C	φ_s	(Mg/m³)
Emulsion + Water										
		0.7			0.404	0.596	0.000	0.000	0.596	1.008
		1.3			0.575	0.425	0.000	0.000	0.425	1.005
		2.0			0.671	0.329	0.000	0.000	0.329	1.003
		2.7			0.730	0.270	0.000	0.000	0.270	1.002
Emulsion + Water + Limestone filler										
0.9		1.3	1.2		0.489	0.361	0.150	0.000	0.511	1.252
0.6		1.3	0.8		0.450	0.332	0.218	0.000	0.550	1.363
0.4		1.3	0.6		0.420	0.309	0.271	0.000	0.580	1.450
0.4		1.3	0.5		0.400	0.295	0.305	0.000	0.600	1.506
0.3		1.3	0.4		0.385	0.284	0.331	0.000	0.615	1.549
0.3		1.3	0.4		0.370	0.273	0.357	0.000	0.630	1.592
0.3		1.3	0.4		0.360	0.265	0.375	0.000	0.640	1.621
0.3		1.3	0.3		0.350	0.258	0.392	0.000	0.650	1.650
0.2		1.3	0.3		0.335	0.247	0.418	0.000	0.665	1.692
0.2		1.3	0.3		0.320	0.235	0.445	0.000	0.680	1.737
0.2		1.3	0.2		0.300	0.221	0.479	0.000	0.700	1.792
Emulsion + Water + Portland cement										
	6.4	1.3		8.5	0.563	0.415	0.000	0.022	0.437	1.049
	2.4	1.3		3.2	0.544	0.400	0.000	0.056	0.456	1.117
	1.5	1.3		2.0	0.525	0.387	0.000	0.088	0.475	1.182
	1.1	1.3		1.4	0.507	0.374	0.000	0.119	0.493	1.244
	0.8	1.3		1.1	0.489	0.360	0.000	0.150	0.511	1.307
	0.5	1.3		0.7	0.450	0.332	0.000	0.218	0.550	1.444
Emulsion + Water + Limestone filler +Portland cement										
1.1	5.4	1.3	1.4	7.2	0.489	0.360	0.128	0.022	0.511	1.261
0.7	3.4	1.3	0.9	4.6	0.450	0.332	0.186	0.033	0.550	1.376
0.5	2.6	1.3	0.7	3.4	0.420	0.310	0.230	0.040	0.580	1.464
0.4	1.9	1.3	0.5	2.6	0.385	0.284	0.281	0.049	0.615	1.567
0.3	1.6	1.3	0.4	2.1	0.360	0.265	0.318	0.056	0.640	1.641

Table 5. Krieger-Dougherty model parameters (Equation 6) obtained for all the tested materials

Dispersion	φ_m	η_0	η_s **(Pa·s)**	$\eta_0\,\varphi_m$	$\mathbf{R^2}$
BW	0.685	1.743	2.58E-03	1.194	0.999
BPW	0.681	1.637	3.14E-03	1.115	0.997
BWF	0.690	1.728	5.32E-03	1.192	0.994
BPWF	0.678	2.132	3.39E-03	1.446	0.967
BWC	0.576	2.037	5.32E-03	1.173	0.975
BPWC	0.574	1.905	5.81E-03	1.094	0.801
BWFC	0.642	1.768	5.32E-03	1.135	0.997
BPWFC	0.641	1.519	1.16E-02	0.973	0.905